Biomedical Optics EXPRESS

Direct visualization and characterization of erythrocyte flow in human retinal capillaries

Phillip Bedggood* and Andrew Metha

Department of Optometry and Vision Sciences, The University of Melbourne, 3010, Australia
**pabedg@unimelb.edu.au*

Abstract: Imaging the retinal vasculature offers a surrogate view of systemic vascular health, allowing noninvasive and longitudinal assessment of vascular pathology. The earliest anomalies in vascular disease arise in the microvasculature, however current imaging methods lack the spatiotemporal resolution to track blood flow at the capillary level. We report here on novel imaging technology that allows direct, noninvasive optical imaging of erythrocyte flow in human retinal capillaries. This was made possible using adaptive optics for high spatial resolution (1.5 μm), sCMOS camera technology for high temporal resolution (460 fps), and tunable wavebands from a broadband laser for maximal erythrocyte contrast. Particle image velocimetry on our data sequences was used to quantify flow. We observed marked spatiotemporal variability in velocity, which ranged from 0.3 to 3.3 mm/s, and changed by up to a factor of 4 in a given capillary during the 130 ms imaging period. Both mean and standard deviation across the imaged capillary network varied markedly with time, yet their ratio remained a relatively constant parameter (0.50 ± 0.056). Our observations concur with previous work using less direct methods, validating this as an investigative tool for the study of microvascular disease in humans.

OCIS codes: (110.1080) Active or adaptive optics; (120.7250) Velocimetry; (170.1470) Blood or tissue constituent monitoring; (170.2655) Functional monitoring and imaging; (170.4470) Ophthalmology.

References and links

1. J. Hirschberg, "Ueber diabetische Netzhautentzündung," Dtsch. Med. Wochenschr. **16**(51), 1181–1185 (1890).
2. R. Gunn, "Ophthalmoscopic evidence of (1) arterial changes associated with chronic renal diseases and (2) of increased arterial tension," Trans. Ophthalmol. Soc. U. K. **12**, 124–125 (1892).
3. N. Patton, T. Aslam, T. Macgillivray, A. Pattie, I. J. Deary, and B. Dhillon, "Retinal vascular image analysis as a potential screening tool for cerebrovascular disease: a rationale based on homology between cerebral and retinal microvasculatures," J. Anat. **206**(4), 319–348 (2005).
4. M. L. Baker, P. J. Hand, J. J. Wang, and T. Y. Wong, "Retinal signs and stroke: revisiting the link between the eye and brain," Stroke **39**(4), 1371–1379 (2008).
5. M. K. Ikram, C. Y. Cheung, T. Y. Wong, and C. P. Chen, "Retinal pathology as biomarker for cognitive impairment and Alzheimer's disease," J. Neurol. Neurosurg. Psychiatry **83**(9), 917–922 (2012).
6. K. M. Rose, T. Y. Wong, A. P. Carson, D. J. Couper, R. Klein, and A. R. Sharrett, "Migraine and retinal microvascular abnormalities: the Atherosclerosis Risk in Communities Study," Neurology **68**(20), 1694–1700 (2007).
7. P. Gasser and J. Flammer, "Blood-cell velocity in the nailfold capillaries of patients with normal-tension and high-tension glaucoma," Am. J. Ophthalmol. **111**(5), 585–588 (1991).
8. H. H. Parving, G. C. Viberti, H. Keen, J. S. Christiansen, and N. A. Lassen, "Hemodynamic factors in the genesis of diabetic microangiopathy," Metabolism **32**(9), 943–949 (1983).
9. G. G. Pietra, F. Capron, S. Stewart, O. Leone, M. Humbert, I. M. Robbins, L. M. Reid, and R. M. Tuder, "Pathologic assessment of vasculopathies in pulmonary hypertension," J. Am. Coll. Cardiol. **43**(12 Suppl S), S25–S32 (2004).
10. J. C. de la Torre, "Is Alzheimer's disease a neurodegenerative or a vascular disorder? Data, dogma, and dialectics," Lancet Neurol. **3**(3), 184–190 (2004).
11. G. J. del Zoppo, G. W. Schmid-Schönbein, E. Mori, B. R. Copeland, and C. M. Chang, "Polymorphonuclear leukocytes occlude capillaries following middle cerebral artery occlusion and reperfusion in baboons," Stroke **22**(10), 1276–1283 (1991).

#175393 - $15.00 USD Received 31 Aug 2012; revised 8 Oct 2012; accepted 13 Nov 2012; published 15 Nov 2012

12. P. Gasser and O. Meienberg, “Finger microcirculation in classical migraine. A video-microscopic study of nailfold capillaries,” Eur. Neurol. **31**(3), 168–171 (1991).
13. H. A. Quigley, “Neuronal death in glaucoma,” Prog. Retin. Eye Res. **18**(1), 39–57 (1999).
14. T. Tanaka, C. Riva, and B. Ben-Sira, “Blood velocity measurements in human retinal vessels,” Science **186**(4166), 830–831 (1974).
15. K. Yaoeda, M. Shirakashi, S. Funaki, H. Funaki, T. Nakatsue, and H. Abe, “Measurement of microcirculation in the optic nerve head by laser speckle flowgraphy and scanning laser Doppler flowmetry,” Am. J. Ophthalmol. **129**(6), 734–739 (2000).
16. B. White, M. Pierce, N. Nassif, B. Cense, B. Park, G. Tearney, B. Bouma, T. Chen, and J. de Boer, “In vivo dynamic human retinal blood flow imaging using ultra-high-speed spectral domain optical coherence tomography,” Opt. Express **11**(25), 3490–3497 (2003).
17. J. Briers, “Laser Doppler and time-varying speckle: a reconciliation,” J. Opt. Soc. Am. A **13**(2), 345–350 (1996).
18. V. J. Srinivasan, H. Radhakrishnan, E. H. Lo, E. T. Mandeville, J. Y. Jiang, S. Barry, and A. E. Cable, “OCT methods for capillary velocimetry,” Biomed. Opt. Express **3**(3), 612–629 (2012).
19. A. Harris, L. Kagemann, and G. A. Cioffi, “Assessment of human ocular hemodynamics,” Surv. Ophthalmol. **42**(6), 509–533 (1998).
20. Y. Wang, B. A. Bower, J. A. Izatt, O. Tan, and D. Huang, “Retinal blood flow measurement by circumpapillary Fourier domain Doppler optical coherence tomography,” J. Biomed. Opt. **13**(6), 064003 (2008).
21. C. E. Riva, J. E. Grunwald, and S. H. Sinclair, “Laser Doppler measurement of relative blood velocity in the human optic nerve head,” Invest. Ophthalmol. Vis. Sci. **22**(2), 241–248 (1982).
22. J. Liang, D. R. Williams, and D. T. Miller, “Supernormal vision and high-resolution retinal imaging through adaptive optics,” J. Opt. Soc. Am. A **14**(11), 2884–2892 (1997).
23. J. A. Martin and A. Roorda, “Direct and noninvasive assessment of parafoveal capillary leukocyte velocity,” Ophthalmology **112**(12), 2219–2224 (2005).
24. J. A. Martin and A. Roorda, “Pulsatility of parafoveal capillary leukocytes,” Exp. Eye Res. **88**(3), 356–360 (2009).
25. J. Tam, P. Tiruveedhula, and A. Roorda, “Characterization of single-file flow through human retinal parafoveal capillaries using an adaptive optics scanning laser ophthalmoscope,” Biomed. Opt. Express **2**(4), 781–793 (2011).
26. J. Tam, K. P. Dhamdhere, P. Tiruveedhula, S. Manzanera, S. Barez, M. A. Bearse, Jr., A. J. Adams, and A. Roorda, “Disruption of the retinal parafoveal capillary network in type 2 diabetes before the onset of diabetic retinopathy,” Invest. Ophthalmol. Vis. Sci. **52**(12), 9257–9266 (2011).
27. R. Chibber, B. M. Ben-Mahmud, S. Chibber, and E. M. Kohner, “Leukocytes in diabetic retinopathy,” Curr. Diabetes Rev. **3**(1), 3–14 (2007).
28. K. Miyamoto and Y. Ogura, “Pathogenetic potential of leukocytes in diabetic retinopathy,” Semin. Ophthalmol. **14**(4), 233–239 (1999).
29. G. W. Schmid-Schönbein, Y. Y. Shih, and S. Chien, “Morphometry of human leukocytes,” Blood **56**(5), 866–875 (1980).
30. B. P. Helmke, S. N. Bremner, B. W. Zweifach, R. Skalak, and G. W. Schmid-Schönbein, “Mechanisms for increased blood flow resistance due to leukocytes,” Am. J. Physiol. **273**(6 Pt 2), H2884–H2890 (1997).
31. Z. Zhong, B. L. Petrig, X. Qi, and S. A. Burns, “In vivo measurement of erythrocyte velocity and retinal blood flow using adaptive optics scanning laser ophthalmoscopy,” Opt. Express **16**(17), 12746–12756 (2008).
32. Z. Zhong, H. Song, T. Y. Chui, B. L. Petrig, and S. A. Burns, “Noninvasive measurements and analysis of blood velocity profiles in human retinal vessels,” Invest. Ophthalmol. Vis. Sci. **52**(7), 4151–4157 (2011).
33. Z. Zhong, G. Huang, T. Y. Chui, B. L. Petrig, and S. A. Burns, “Local flicker stimulation evokes local retinal blood velocity changes,” J. Vis. **12**(6), 3 (2012).
34. P. Bedggood and A. Metha, “Variability in bleach kinetics and amount of photopigment between individual foveal cones,” Invest. Ophthalmol. Vis. Sci. **53**(7), 3673–3681 (2012).
35. F. C. Delori, R. H. Webb, and D. H. Sliney; American National Standards Institute, “Maximum permissible exposures for ocular safety (ANSI 2000), with emphasis on ophthalmic devices,” J. Opt. Soc. Am. A **24**(5), 1250–1265 (2007).
36. R. D. Frostig, E. E. Lieke, D. Y. Ts’o, and A. Grinvald, “Cortical functional architecture and local coupling between neuronal activity and the microcirculation revealed by in vivo high-resolution optical imaging of intrinsic signals,” Proc. Natl. Acad. Sci. U.S.A. **87**(16), 6082–6086 (1990).
37. B. Falsini, C. E. Riva, and E. Logean, “Flicker-evoked changes in human optic nerve blood flow: relationship with retinal neural activity,” Invest. Ophthalmol. Vis. Sci. **43**(7), 2309–2316 (2002).
38. J. Tam, J. A. Martin, and A. Roorda, “Noninvasive visualization and analysis of parafoveal capillaries in humans,” Invest. Ophthalmol. Vis. Sci. **51**(3), 1691–1698 (2010).
39. P. Bedggood and A. Metha, “Oximetry imaging of the retinal microvasculature using adaptive optics,” in *Association for Research in Vision and Ophthalmology Annual Meeting* (Fort Lauderdale, FL, 2012).
40. R. Keane and R. Adrian, “Theory of cross-correlation analysis of PIV images,” Appl. Sci. Res. **49**(3), 191–215 (1992).
41. S. Wolf, O. Arend, H. Toonen, B. Bertram, F. Jung, and M. Reim, “Retinal capillary blood flow measurement with a scanning laser ophthalmoscope. Preliminary results,” Ophthalmology **98**(6), 996–1000 (1991).
42. A. G. Hudetz, “Blood flow in the cerebral capillary network: a review emphasizing observations with intravital microscopy,” Microcirculation **4**(2), 233–252 (1997).
43. M. Iwasaki and H. Inomata, “Relation between superficial capillaries and foveal structures in the human retina,” Invest. Ophthalmol. Vis. Sci. **27**(12), 1698–1705 (1986).

#175393 - $15.00 USD Received 31 Aug 2012; revised 8 Oct 2012; accepted 13 Nov 2012; published 15 Nov 2012

44. Y. C. Fung, "Stochastic flow in capillary blood vessels," Microvasc. Res. **5**(1), 34–48 (1973).
45. P. C. Johnson and H. Wayland, "Regulation of blood flow in single capillaries," Am. J. Physiol. **212**(6), 1405–1415 (1967).
46. G. Pawlik, A. Rackl, and R. J. Bing, "Quantitative capillary topography and blood flow in the cerebral cortex of cats: an in vivo microscopic study," Brain Res. **208**(1), 35–58 (1981).
47. A. Villringer, A. Them, U. Lindauer, K. Einhäupl, and U. Dirnagl, "Capillary perfusion of the rat brain cortex. An in vivo confocal microscopy study," Circ. Res. **75**(1), 55–62 (1994).
48. Y. C. Fung, "Blood flow in the capillary bed," J. Biomech. **2**(4), 353–372 (1969).
49. D. Cousineau, C. P. Rose, D. Lamoureux, and C. A. Goresky, "Changes in cardiac transcapillary exchange with metabolic coronary vasodilation in the intact dog," Circ. Res. **53**(6), 719–730 (1983).
50. I. Krolo and A. G. Hudetz, "Hypoxemia alters erythrocyte perfusion pattern in the cerebral capillary network," Microvasc. Res. **59**(1), 72–79 (2000).
51. M. L. Schulte, J. D. Wood, and A. G. Hudetz, "Cortical electrical stimulation alters erythrocyte perfusion pattern in the cerebral capillary network of the rat," Brain Res. **963**(1-2), 81–92 (2003).
52. J. Vogel and W. Kuschinsky, "Decreased heterogeneity of capillary plasma flow in the rat whisker-barrel cortex during functional hyperemia," J. Cereb. Blood Flow Metab. **16**(6), 1300–1306 (1996).
53. S. N. Jespersen and L. Østergaard, "The roles of cerebral blood flow, capillary transit time heterogeneity, and oxygen tension in brain oxygenation and metabolism," J. Cereb. Blood Flow Metab. **32**(2), 264–277 (2012).
54. H. K. Rucker, H. J. Wynder, and W. E. Thomas, "Cellular mechanisms of CNS pericytes," Brain Res. Bull. **51**(5), 363–369 (2000).
55. S. S. Segal, "Regulation of blood flow in the microcirculation," Microcirculation **12**(1), 33–45 (2005).
56. M. M. Guest, T. P. Bond, R. G. Cooper, and J. R. Derrick, "Red Blood Cells: Change in Shape in Capillaries," Science **142**(3597), 1319–1321 (1963).
57. F. Grubbs, "Procedures for detecting outlying observations in samples," Technometrics **11**(1), 1–21 (1969).
58. D. Cook, "Detection of influential observations in linear regression," Technometrics **19**(1), 15–18 (1977).

1. Introduction

The eye is the only organ in the body where the deep internal vasculature can be observed directly, noninvasively and in high resolution. Correlation between abnormalities in the retinal vasculature and abnormalities elsewhere in the body have been demonstrated in a diverse array of conditions including diabetes [1], hypertension [2], stroke [3,4], Alzheimer's disease [3,5], migraine [6] and glaucoma [7]. Each of these conditions manifests pathology in the microvasculature [8–13], which is the primary site of exchange between blood and tissue. Measurement of retinal blood flow, especially at the level of the microvasculature, therefore offers a unique advantage for the longitudinal study of vascular disease in humans.

Several techniques have become well established for the noninvasive measurement of blood flow in the human retina. These include laser Doppler flowmetry [14], laser speckle contrast imaging [15] and Doppler OCT [16]. These methods all rely on the relationship between the velocity of red blood cells and the changes in frequency imparted to light that is scattered from them [17]. These techniques provide repeatable measures of blood flow in the larger retinal vessels, but suffer from limited spatial and temporal resolution as well as low signal to noise ratio for vessels oriented more perpendicularly to the probe beam [18–20]. Erythrocyte scatter also obfuscates the relationship between the frequency and velocity spectrum, limiting the ability to measure absolute velocities via such indirect approaches [14]. These issues render the above techniques ineffective for study of the microvasculature, although some approximations have been made [18,21].

The required spatial resolution to image the microvasculature can be achieved using adaptive optics, a technology that reshapes the optical wavefronts emanating from the eye [22] to achieve diffraction-limited resolution (<2 μm). This is more than sufficient for visualization of the smallest retinal capillaries (~5 μm diameter). Previous work using adaptive optics scanning laser ophthalmoscopy (AOSLO) has taken advantage of the rarity of leukocytes in the blood stream to track them individually and so quantify flow [23]. This approach revealed marked variability in leukocyte velocity and pulsatility, between capillaries and between subjects, in normal retina [24]. The most direct, or thoroughfare, capillaries were seen to account for ~2/3 of all leukocyte traffic [25]. Thoroughfare capillaries were shown to preferentially undergo morphological changes in pre-clinical diabetic retina, leading to leukocytes being redistributed to exchange capillaries [26] and confirming recent evidence of leukocyte-based microvascular disruption in diabetes [27,28].

#175393 - $15.00 USD Received 31 Aug 2012; revised 8 Oct 2012; accepted 13 Nov 2012; published 15 Nov 2012

Although useful to study in its own right, leukocyte flow is not a good surrogate for erythrocyte flow due to the former's larger size, reduced deformability [29] and relative rarity in the blood [30]. Erythrocyte flow has its own obvious importance in disease processes as the carrier of oxygen to tissue. Erythrocyte flow in capillaries was not able to be measured unambiguously in previous adaptive optics work due to limitations in spatial and temporal resolution [25]. An alternate approach in which the scanning raster of an AOSLO is fixed in one dimension has allowed precise measurements to be made along the cross-section of larger vessels ~30-100 μm in diameter [31]. This has allowed the flow profile to be characterized in these vessels, as well as changes to be measured resulting from the cardiac cycle [32] and from visual stimulation of the retina [33]. However this technique is also not suited to study of erythrocyte flow in the microvasculature.

To directly visualize erythrocytes in retinal capillaries we combined the spatial resolution afforded by adaptive optics, the temporal resolution of a fast sCMOS camera, and a supercontinuum laser that allows us to selectively deliver imaging light that is strongly absorbed by hemoglobin. While confocal AOSLO systems typically focus on an intermediate position between the capillary bed and the photoreceptor mosaic to aid image registration, our flood-based ophthalmoscope is able to accurately register data while focused directly on the capillary bed. This overall approach allows us to directly and unambiguously visualize the flow of individual erythrocyte packets, separated by plasma gaps, in the retinal capillaries. This direct visualization of spatiotemporally dense and high contrast moving particles lends itself to particle image velocimetry (PIV), which was used to quantify erythrocyte flow.

We provide details here on our methodology, the adaptation of standard PIV approaches to suit our data, and validation of measured velocities against a noisy phantom data set. We use our approach to report on the statistics of normal erythrocyte velocity and velocity fluctuations both within and across capillaries in a normal human subject.

2. Methods

The subject, who is also the first author, was a healthy, nonsmoking, 29 year old male with no ocular pathology or significant refractive error. The project was carried out in accordance with the tenets of the Declaration of Helsinki, and approved by the University of Melbourne Human Ethics Committee.

2.1. Adaptive optics imaging

The imaging system is a flood adaptive optics ophthalmoscope that has been described elsewhere [34], with the exception that the retinal camera is now an Andor NEO sCMOS device (Andor Technology PLC, Belfast, UK). The main functional difference brought about by this change is the much greater frame rate. It is also somewhat more sensitive, with peak sensitivity at 600 nm (0.57 quantal efficiency). The device operates in two distinct shutter modes: rolling and global. Rolling shutter produces a staggered exposure between adjacent pixel rows (10 μs delay between each row) which allows the frame rate to be doubled in most cases. This staggered exposure was deemed unsuitable for monitoring of blood flow in 2 dimensions due to the high flow velocity, and we instead used global shutter which exposes all pixels simultaneously. The device is capable of a sustained 50 fps at full frame (2560 x 2160) using global shutter, however the frame rate can be greatly increased by restricting the region of interest in the vertical direction, due to the way in which data is read out from the sensor. We limited the vertical extent to 200 pixels (70 μm) to achieve a frame rate of 460 fps for this work. It was not necessary to update the adaptive optics correction during the acquisition of our sequences, which were 60 frames (130 ms) in length.

The sCMOS camera outputs a digital signal indicating the beginning of each frame exposure. This output was used to trigger our imaging source, producing a train of exposures each 1.07 ms long. As previously described [34], our imaging source is a supercontinuum laser that is passed through acousto-optic tunable filters to select narrow wavebands of interest for imaging, and then through 32 m of multimode fiber to minimize speckle. In this work we selected wavebands centered on 593 nm. This provided near-optimal erythrocyte contrast,

#175393 - $15.00 USD Received 31 Aug 2012; revised 8 Oct 2012; accepted 13 Nov 2012; published 15 Nov 2012

taking into account the variance with wavelength of both the maximum permissible exposure (MPE) [35] and the output of our laser. Power at the cornea was 0.5 mW, which is ~35 times below the MPE for each 130 ms imaging sequence according to ANSI guidelines [35]. 5 imaging sequences were acquired in the same area and presented for analysis in this work.

Functional imaging of the cortex has shown changes in capillary flow to occur as quickly as 400 ms after the onset of neuronal activity [36]. Our 130 ms acquisition time is therefore anticipated to be too short for a metabolic effect to occur as a result of neuronal stimulation by the imaging light. Changes in inner retinal flow are also known to be greatly reduced at high flicker rates [37], such as that of our imaging light.

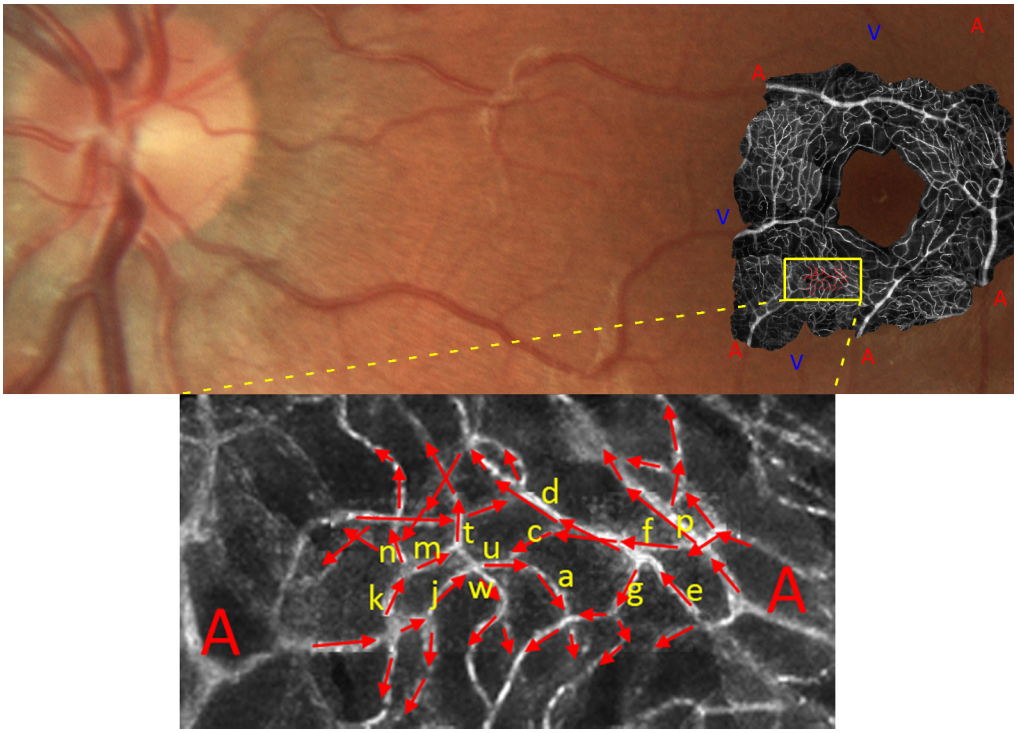

Fig. 1. Area of analysis. Top: Conventional fundus image (color) overlaid with an adaptive optics montage of the capillary network surrounding the foveal avascular zone (grayscale). A, V denotes arteries and veins. Bottom: Shows inset demarcated by yellow border in top. Arrows indicate direction of erythrocyte flow. Lower case letters denote capillary segments discussed in the text below. This is a region of high confluence, with 2 neighboring arterioles (A) delivering blood in opposing directions.

2.2. Imaged area

Figure 1 shows a conventional retinal fundus photograph from our subject (color), registered with a motion-contrast enhanced [38] montage of the parafoveal capillary network obtained at 593 nm, using our previous camera at 12 fps [39]. Approximately 100 frames were acquired at each 1.1° diameter area to create the montage. Arterioles (A) and venules (V) are indicated on the figure. These were identified based on color and tracking of branches from the optic nerve head, and confirmed by observing the direction of flow in our sequences. The highlighted box and corresponding inset indicates the area that was analyzed in this work, which is close to the edge of the foveal avascular zone. This provided a capillary bed that was predominantly mono-stratified (to within ~0.1 D, or 35 μm) according to subjective judgment of capillary focus with our system; stepping the focus through the entire retinal thickness did not reveal any additional vessels beyond this layer at this retinal location. The area chosen is also a highly chaotic zone in which 2 nearby arterioles deliver supply from opposite directions; the

#175393 - $15.00 USD Received 31 Aug 2012; revised 8 Oct 2012; accepted 13 Nov 2012; published 15 Nov 2012

area displayed many sharp branch points and sudden changes in velocity. The direction of flow in each capillary segment (red arrows) was determined both subjectively and using PIV analysis (below), which were in excellent agreement.

2.3. Image registration

After acquisition of image sequences, background noise was subtracted from the raw images. These were then divided by a flat-field image, which was generated by collecting several hundred frames of data at the same wavelength, at a slower frame rate, in which the subject was instructed to move fixation erratically.

Image sequences were registered using cross-correlation with sub-pixel accuracy. Prior to registration, images were filtered in Fourier space to reduce noise, using a bandpass filter that masked spatial details <0.7 μm or >18 μm in size. This filter was tapered using a raised-cosine function (peaking at 1 in the image center and trailing to 0 at the edge) to reduce the introduction of artifacts in the spatial image. Correction for angular rotation was necessary in our previous work at lower frame rate [34], but was not necessary with the current frame rate and short overall imaging time. Note that filtering was used only to determine correct image registration; final data sequences for PIV analysis were not filtered in this way.

The above procedure was sufficient to provide high quality registration with the focus at the level of the inner retinal capillaries, i.e. with minimal reliance on the underlying cone mosaic.

2.4. Enhancement of erythrocyte motion

The static contrast of capillaries and erythrocytes, relative to background tissue, was low. This is illustrated in Fig. 2 (top), which shows a raw frame from one of our data sequences. PIV approaches typically make use of a high contrast tracer particle [40] that can easily be divorced from the surrounding media; an analogue for measurement of retinal flow is fluorescein angiography [41], however this is an invasive technique. Fortunately the moving erythrocytes in our sequences produced large changes in contrast over time; this is best appreciated in the sequence Fig. 2 (Media 1), or by the "division" image analysis [38] of the same sequence in Fig. 2 (bottom). A useful, direction-preserving method to accentuate such changes in the context of PIV was to subtract the first principal component from each pixel, using time as a variable. This was found to greatly eliminate static structural information while leaving erythrocyte motion intact; we filtered each data sequence in this way before analysis.

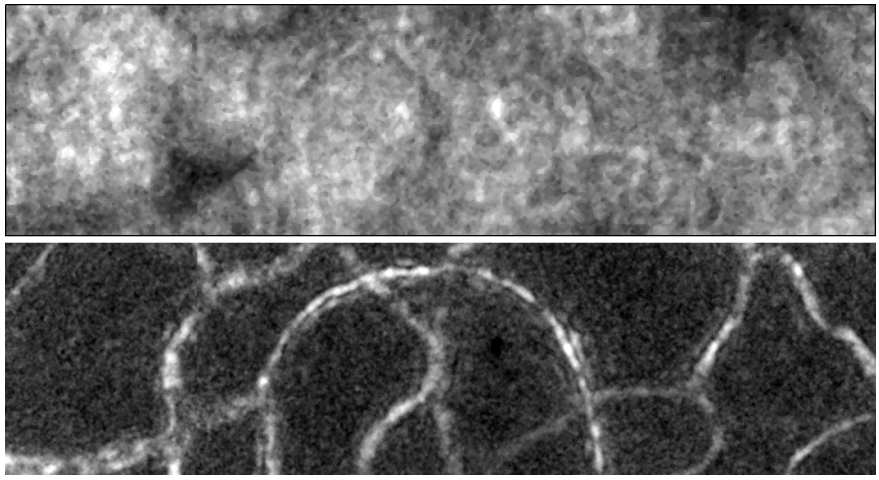

Fig. 2. Sample of our imaging data. Top: a single frame at 593 nm, 1° nasal and 2° inferior to the foveal center, close to the edge of the foveal avascular zone. Bottom: Motion contrast enhancement of the same area, based on 60 frames of data (130 ms). The sequence itself is shown in Media 1.

#175393 - $15.00 USD Received 31 Aug 2012; revised 8 Oct 2012; accepted 13 Nov 2012; published 15 Nov 2012

Another possible approach to enhance erythrocyte contrast would be to use multiple wavelengths to exploit the spectral absorption signature of hemoglobin, but we have previously found this to be of dubious reliability at the capillary level when viewed *in vivo* [39]. This approach is presumably frustrated by complex interference and scattering effects which outweigh wavelength-selective absorption in single erythrocytes, which are individually of low optical density.

2.5. Particle image velocimetry

In PIV, each frame of the sequence is divided into small regions of interest (ROIs) and cross-correlated with a larger surrounding ROI from the previous frame [40]. The displacement of the peak of the cross-correlation function indicates the ensemble motion of particles present within the region. Larger ROIs correspond to faster maximum measurable velocity, while smaller ROIs correspond to better spatial resolution; the latter is important for measuring velocity changes along a vessel, while avoiding the influence of nearby vessels and crossing points. It is therefore important to select the ROI size based on known physiological constraints [40]. It is possible to expand the range of measurable velocities by employing search boxes of varying size, however this requires that a method be devised to select the most appropriate measurement at each position in the image.

It is apparent that there is no fixed ideal set of parameters for PIV analysis; the parameters reported here were chosen using trial and error to empirically maximize accuracy when applied to a known, noisy ("phantom") data set—see section 2.6 below. Each step in the algorithm was found to be useful in defeating a particular sub-class of errors in the phantom data set. The maximum velocity measurable was beyond the range of physiologically relevant capillary velocities [24,25,42], to ensure that no data was lost as a result of insufficient ROI size. The final parameters of our algorithm were as follows:

Minimum velocity: 1.5 pixels/frame (0.24 mm/s)

Maximum velocity: 15, 25, or 30 pixels/frame (2.4, 4.0, 4.8 mm/s)—3 separate analyses

Small ROI size: 32 pixels (11. 2 x 11.2 μm)

Large ROI size: 48, 80 or 96 pixels (17, 28 or 34 μm)—chosen based on max. velocity

Since the axis of motion at each point on a capillary cannot change, we arrived at an overall direction of motion for each sample point by taking the median flow angle over an image sequence. Vectors more than 30° from this value were rejected as noise-evoked outliers, and the median angle of the remaining vectors taken again. To determine speed, these vectors were projected onto the direction found above, and the median of the resulting lengths was taken. A minimum of 6 measurements were required for a point to be considered valid data, to minimize background noise. The final array of flow vectors was passed through a 2D median filter, which further suppressed background noise. This stringent approach had the disadvantage that no data was recorded for some capillary segments.

To determine how velocity varied over shorter time scales we employed a rolling temporal window of 15 frames (33 ms) duration, which is equivalent to passing the velocity signal through a lowpass filter. The same procedure as above was applied, however the initial direction of motion as determined for all frames was used as the starting direction. This greatly assisted in correctly rejecting spurious motion in this much smaller number of measurements, however, it did leave the algorithm blind to any rapid reversals in motion. Visual inspection of our data did not reveal any reversals to occur, and if they did, these would be visible as gaps in the velocity trace for a given capillary segment.

Analysis with three different maximum velocities was used to increase the range of valid measurable velocities. A robust method to select the most appropriate velocity, determined empirically (see below), was to simply accept the fastest of the 3 measurements.

#175393 - $15.00 USD Received 31 Aug 2012; revised 8 Oct 2012; accepted 13 Nov 2012; published 15 Nov 2012

2.6. Phantom data set

We generated a model, or phantom, data set to allow us to empirically determine a robust approach for velocity estimation from quantifiably noisy data. We used software to construct an imaging field of the same nominal size, consisting of straight, invisible "vessels" oriented in various directions on a white background. Each vessel was populated with black rectangular "erythrocyte" packets (5.0 x 12 μm in dimension), with a 12 μm gap between each packet. In succeeding frames of the phantom sequence these packets were propagated at constant speed along each vessel, with the speed for different vessels chosen to span the known physiological range of capillary velocities [24,25,42]. To each pixel of each binary frame was added a sufficient level of white noise such that the PIV approach of section 2.5 rejected a similar percentage of frame pairs as for our actual image data. In this way we regarded the phantom set as being sufficiently degraded in image quality so as to mimic the real data.

Figure 3 (grayscale) shows a single frame from a phantom data sequence, while the colored arrows show the PIV analysis for the entire 60 frame sequence. Both arrow color and length indicate the measured velocity. Points devoid of coloured arrows did not pass the acceptability criteria described in section 2.5; i.e. the data was not differentiated from noise. The numbers listed over each vessel segment show median velocity ± median absolute difference of the line of points closest to the center of each vessel. The numbers in parantheses indicate the true (input) velocity. Measurements close to a crossing point were ignored. There were a minimum of 10 readings for each vessel. The error rate ranged from 0 to 7% from the true velocity, confirming the robustness of this approach in the face of a noisy data set. We are therefore confident to state that, away from branch and crossing points, our margin for error in measured velocity in our actual imaging sequences is <10%.

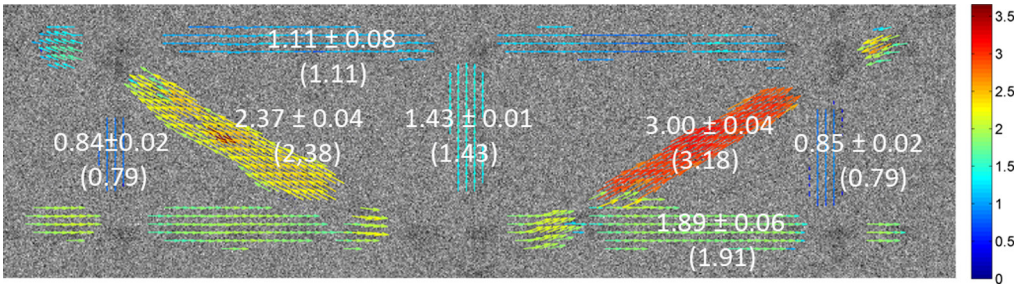

Fig. 3. Phantom data set for validation of measured velocities, consisting of 7 modeled capillaries. Grayscale: a single frame from the phantom data sequence. Modeled erythrocyte clusters are visible as dark rectangular patches. Color overlay: Velocity vectors in each region of interest. Speed is denoted both by arrow length and color. Numbers: median velocity ± median absolute difference (true velocity). Units are mm/s. Velocity measurements were derived by considering a line of points (minimum 10 per vessel) that were closest to the vessel center.

2.7. Reporting of velocity

A potential limitation of our measurements is that motion is only measured transversely in the retina (i.e., along the surface of our detector) as opposed to along the true capillary detection, which may contain an axial component. This is a minor limitation because most capillaries are oriented almost entirely transversely in the retina [43], and strong exceptions to this rule should be readily apparent from our sequences by changes in erythrocyte packet length along a given capillary. It was not possible to detect any such changes in the area that we imaged here.

It should be noted that even though data is reported only for a single subject, the large number of erythrocytes contributing to each velocity measurement in each capillary afford good reliability compared with leukocyte tracking methods [24,25] which rely on a smaller number of samples due to the scarcity of leukocytes in the blood stream.

#175393 - $15.00 USD Received 31 Aug 2012; revised 8 Oct 2012; accepted 13 Nov 2012; published 15 Nov 2012

Measurements of particle displacement were converted into absolute distances by adjusting for measured axial length of the subject's eye, which was 23.97 mm. This was measured with an Axis II ultrasound device (Quantel Medical, Clermont-Ferrand, France).

3. Results

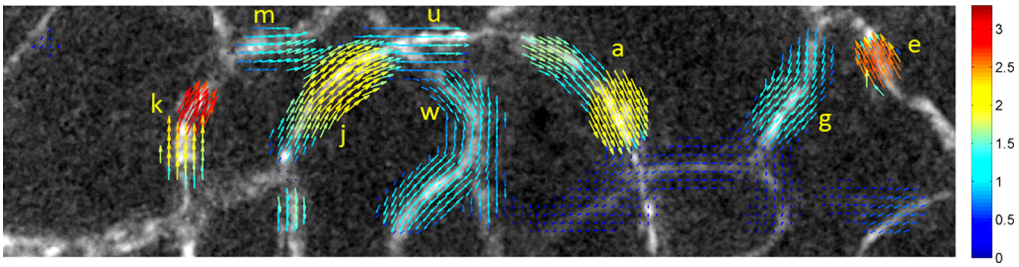

Fig. 4. PIV analysis (median velocity) from the same image sequence as in Fig. 2 (Media 1). Imaging wavelength was 593 nm, imaged area was 1° nasal and 2° inferior to the foveal center. Diameter of displayed region is ~0.8 x 0.2°. Grayscale: motion contrast enhanced "division" image [38] from this sequence. Color arrows: Velocity vectors in each region of interest. Speed is denoted both by arrow length and color. Letters: Labeled capillary segments referred to in the text; labels correspond to those in Fig. 1.

Figure 4 shows the median velocity over the course of the same data sequence from Fig. 2 (Media 1). Velocity is represented both by arrow length tangential to the vessel orientation, and by arrow color. Spatial variability was high even over the small area shown (~0.8 x 0.2°), with erythrocyte velocities ranging from ~0.5-3.1 mm/s across space in this sequence. The variability can be further appreciated in Fig. 2 (Media 1).

It is instructive to divide the capillaries into segments; we defined a length of vessel as a capillary segment if it consisted of at least 5 data points along the vessel that were unbroken by missing data or a branch/crossing, and in which single file erythrocyte flow was subjectively apparent. We noted cases of marked variability along several capillary segments, including between consecutive segments where no branching had occurred. For example, in Fig. 4, segment **u** shows markedly reduced velocity compared to the upstream and downstream segments **j** and **a**. This behavior is assumedly a result of the crossing vessels bounding segment **u**. It is also interesting to note the downstream increase in speed along segment **a**, which must indicate either widening of the capillary segment, or erythrocytes "catching up" to the less impeded [44] flow of plasma. In a separate sequence (not shown), instead segment **u** maintained a relatively constant velocity (1.55 ± 0.09 mm/s), while the surrounding segments were far more variable (1.51 ± 0.48 and 1.23 ± 0.32 mm/s for **j** and **a**). In other words, in that sequence segment **u** was likely buffered against changes in velocity by traffic in the crossing segments.

Figure 5 shows the standard deviation in velocity over the course of a sequence that showed high temporal variability. Arrow length and color both denote the standard deviation in velocity, with each individual time point incorporating 15 frames of data as explained above. The variability inherent in this sequence can be further appreciated in Fig. 5 (Media 2), which shows the original data sequence together with an overlay of the rolling temporal PIV analysis. Flow in the entire capillary network in this area can be seen to increase dramatically over the course of the sequence. To derive an overall velocity measure for each capillary segment, we took the median of all data points that lay along the vessel and were oriented along the apparent vessel direction on the motion contrast image. Figure 6 shows the result of this analysis, in which the velocity in each segment is seen to ramp up throughout the duration of the sequence. It is worth noting that velocity in consecutive segments **u** and **a** (plotted in red) increased dramatically, but with the change in downstream segment **a** preceding upstream segment **u** by some 40 ms. This presumably corresponds to upstream "traffic" in the venous direction that has caused a back-propagation of resistance up the vessel.

#175393 - $15.00 USD Received 31 Aug 2012; revised 8 Oct 2012; accepted 13 Nov 2012; published 15 Nov 2012

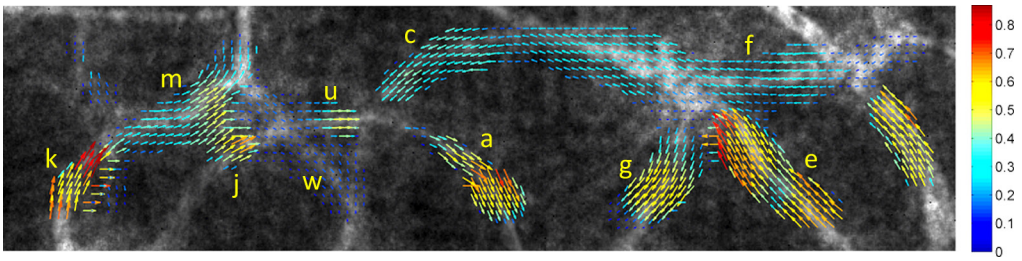

Fig. 5. PIV analysis (standard deviation) from an image sequence showing marked variability of flow over time, as well as location. The corresponding sequence is shown in Media 2. Grayscale: motion contrast enhanced "division" image [38] from this sequence. Color arrows: Standard deviation of velocity in time, using temporal windows 15 frames (33 ms) long. Standard deviation is denoted both by arrow length and color. Letters: Labeled capillary segments referred to in the text; labels correspond to those in Fig. 1.

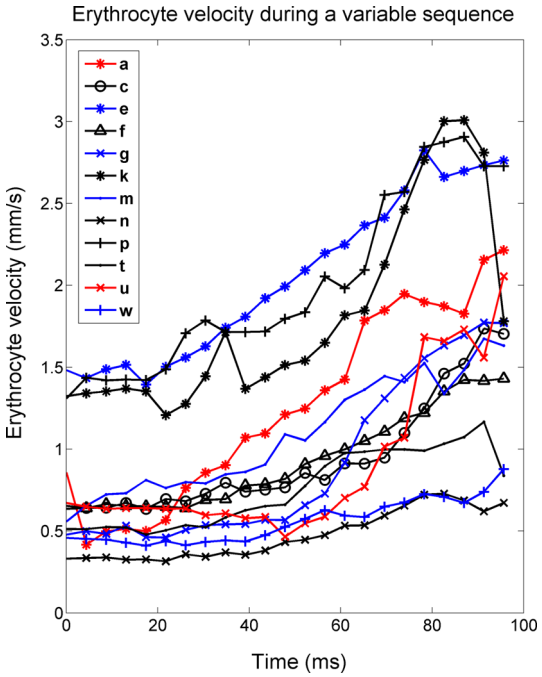

Fig. 6. Velocity in each capillary segment in the same image sequence shown in Fig. 5 (Media 2). Velocity generally increased throughout the course of this sequence. Blue plots indicate capillary segments **e**, **g**, **m** and **w** that were present in all sequences, and are analyzed in Fig. 7. Red plots indicate segments **a** (asterisks) and **u** (crosses), which are consecutive and are referred to in the text.

The global correlation in velocity evident in Fig. 6 was not apparent in the other sequences. To illustrate this, Fig. 7 shows the velocity plots for each of the 4 segments plotted in blue in Fig. 6. These segments (**e**, **g, m** and **w**) were visible in all 5 sequences analyzed. Each panel of Fig. 7 corresponds to a segment, and each plot to a data sequence. Of interest is that a) a given capillary segment was able to have a diverse array of mean velocity and variability in velocity; b) in the same image sequence some capillaries changed velocity markedly while others remained highly constant; and c) during the sequence of generally increasing velocity, the segments did not all increase their velocity at the same time.

Although we have presented data here only from selected sequences that provide the most clear and illustrative examples, interested readers may obtain the entirety of our velocity data upon request.

#175393 - $15.00 USD Received 31 Aug 2012; revised 8 Oct 2012; accepted 13 Nov 2012; published 15 Nov 2012

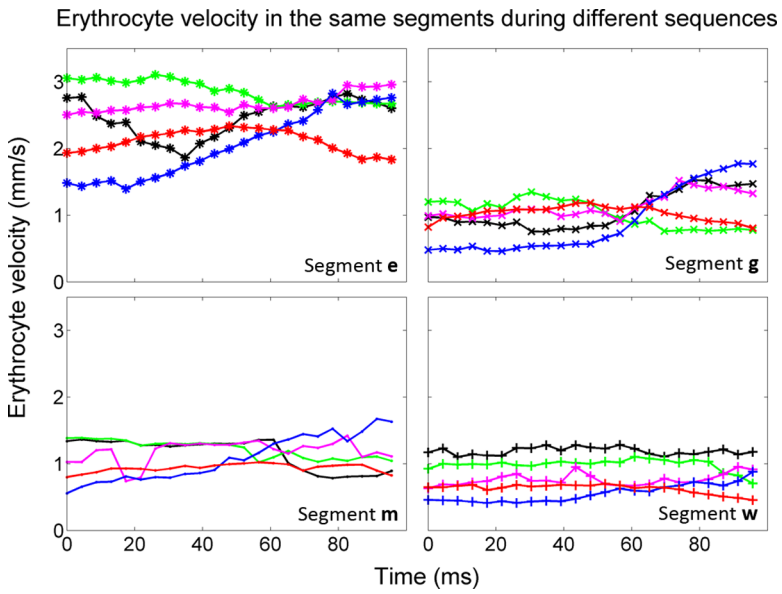

Fig. 7. Velocity in the same 4 capillary segments across 5 image sequences. Each panel corresponds to the same capillary segment, and each plot color corresponds to the same image sequence.

4. Discussion

We have demonstrated and validated a technique that allows direct, noninvasive visualization of erythrocyte packets flowing in single file through capillaries in the living human retina. The range of erythrocyte velocities in the measured area (0.3–3.3 mm/s range, mean 1.3 mm/s) agrees well with previously published figures for retinal leukocytes in humans [24,25] and for cerebral erythrocytes in animals (see [42] for review). Our observation of marked variability in the distribution of erythrocyte velocities across space and time also echoes observations made by others [45–47].

Additional observations of interest, noted above, included: the potential for global velocity in the imaged area to correlate between all capillary segments, which was likely related to cardiac activity; slowing and buffering of changes to flow resulting from contact by neighbouring capillaries, which was likely due to compressive effects on the capillary lumen; variations in velocity along capillary segments in the absence of any branching, due either to alterations in resistance along short lengths of a capillary or to differences between plasma and erythrocyte velocity; and changes in velocity propagating upstream in a vessel, likely due to downstream "traffic".

Passive fluctuations in capillary flow are thought to occur as a result of interaction between the vessels (geometry, redundancy and compliance) and the stochastic variations that occur in the number and size of erythrocytes [44,46,48]. This causes large fluctuations to occur at rates that are not readily comparable to the heart or respiration rates—full range fluctuations have been noted to occur as quickly as 40-90 Hz [46], or as slow as 0.1 Hz [45]. In other words, although heart and respiration rates are an important source of variability in capillary velocity [25], it is by no means a straightforward relationship; large amounts of data are potentially required to meaningfully characterize mean velocity or pulsatility of each capillary. This somewhat limits the usefulness of analyzing the flow dynamics of any single capillary.

A more practical approach may be to analyze the overall network properties of the capillary plexus in a given location. Mounting evidence suggests that the heterogeneity of flow in the capillary network is adjusted based on the metabolic needs of the tissue, with flow

#175393 - $15.00 USD Received 31 Aug 2012; revised 8 Oct 2012; accepted 13 Nov 2012; published 15 Nov 2012

being redistributed to more homogeneous patterns under metabolic challenge [42,47,49–52]. Modeling predicts this redistribution to significantly improve metabolite exchange with tissue, especially oxygen extraction [53]. Redistribution of flow may result from constriction/dilation of pericytes [54] or pre-capillary arterioles [55]. If capillary heterogeneity is indeed linked to metabolic needs, a useful measure of heterogeneity should vary little in a given retinal location under the same adaptation and environmental conditions, as in our experiment. Comparing instantaneous velocity for the imaged capillary network across all time points in our sequences, mean network velocity was 1.33 ± 0.28 mm/s, while standard deviation in network velocity was 0.65 ± 0.12 mm/s. However the ratio of these parameters (standard deviation / mean) was more constant with time (0.50 ± 0.056). This implies that under constant metabolic need, transient increases in network velocity are accompanied by commensurate increases in the variability between capillary segments. Further work is currently underway to establish the range of normative values for capillary heterogeneity in healthy subjects both at baseline and under metabolic activity (e.g. hypoxia/hypercapnia and functional stimulation). This will allow comparisons to be made to cases of vascular disease, to learn how baseline and autoregulatory dynamics in flow may be compromised at the capillary level.

The rules governing division of flow at capillary branches are of interest. If it is assumed that the local haematocrit does not change significantly after a branch, Kirchoff's circuit law suggests that the velocity prior to the branch should be the sum of the velocities after the branch. This was observed to be the case in certain vessels; for example, segment **e** branches into segments **d** and **g**, with the component velocities summing to within 1% of **e** in one sequence and within 10% in another sequence. However this assumption was violated in other segments; for example in one sequence the branches **m** and **n** from segment **k** gave only 70% of the total velocity of segment **k**. Therefore it is apparent that the local haematocrit must be allowed to vary between branches, as has been reported by others [47,50,51]. This result is expected from theory—in fact, in the absence of stochastic variations in erythrocyte size and position within the capillary, all erythrocytes would follow the branch offering the lowest resistance [44]. Variations in haematocrit mean that measurement of velocity alone is insufficient to completely characterize the dynamics of capillary flow. It should be possible for local haematocrit data to be extracted from our sequences, for example by counting intensity minima passing each point along a capillary. There is still some uncertainty in this approach, since the number of erythrocytes comprising each packet is not known (see below). For this reason a more practical measure may be to simply quantify the proportion of a capillary segment that is occupied by erythrocytes.

We cannot state whether each and every moving erythrocyte packet in our sequences (e.g. see Fig. 2, Media 1) is a single erythrocyte, or a small number of erythrocytes traveling in apposition. Erythrocyte diameter is ~8 μm when not being forced through the capillary bed, while measured packet length was ~10-12 μm. Erythrocytes are known to lengthen somewhat in the capillaries [56], as a result of their relatively liquid center [48] and the ~5 μm capillary diameter. It should also be noted that we expect some artifactual enhancement of apparent packet length due to motion blur over our ~1 ms exposure time, on the order of ~0.5-3 μm according to our measured range of erythrocyte speeds. Given these considerations, it would be instructive to quantify erythrocyte packet length in different capillary segments. In practice to date, we have found this difficult because a given packet often changes in appearance between high and low contrast as it traverses the capillary bed. This could result from changes in specular reflection as the deformable packet conforms to the shape of the capillary wall, or from interference between the anterior and posterior faces of the capillary wall (which are only 5 μm apart and so within the ~7 μm coherence length of our imaging light source [34]). Thus our rough estimate of packet length stems from a relatively small number of packets, taken between adjacent frames where the packet appearance remained at high contrast. We have therefore presented results here only for analysis of packet velocity, to which the PIV method is well suited.

#175393 - $15.00 USD Received 31 Aug 2012; revised 8 Oct 2012; accepted 13 Nov 2012; published 15 Nov 2012

A primary limitation to consider for this technique is the relatively short imaging wavelength that was used to maximize erythrocyte contrast (593 nm), compared to the longer wavelengths that are more typically used to enhance patient comfort and reduce the risk of light exposure damage. To determine whether such a short imaging wavelength was truly necessary, we repeated our imaging procedure using 720 nm light. Dark, moving erythrocyte packets were still apparent, with reduced signal to noise ratio, such that our PIV algorithm obtained useful velocity measures in only ~1/2–2/3 of capillary segments compared with 593 nm. The 720 nm data was also much more sensitive to small changes in image quality. Despite the reduced signal to noise ratio, contrast was in fact much higher than expected based solely on the ratio of hemoglobin absorption between these wavelengths, which is more than an order of magnitude. This suggests that scatter and/or interference [39] effects dwarf the absorption of light due to hemoglobin alone, when imaging individual erythrocyte packets in the capillaries. This limits the measurement of hemoglobin content via spectral means in these smallest of vessels. For the purposes of improving contrast for velocity measurement, any interference present may be enhanced by increasing the spatial coherence (confining the illumination delivery within the pupil) and the temporal coherence (reducing the bandwidth) of the illumination.

It is worth noting that after the desired focus was set, all acquired sequences were used for analysis. Thus the PIV method did not seem to have any stringent image quality requirement over and above the typical AO imaging work that we have undertaken in the past [34,39]. In other words, efficiency of data collection was high, which mitigates concerns about the somewhat lower MPE at 593 nm. To further mitigate these concerns we allowed an average of 2-3 minutes to elapse between acquisition of each sequence. To achieve more efficient data collection in a larger number of subjects, it may be prudent to acquire sequences from each desired retinal eccentricity in series, repeating this entire process as many times as desired, to further minimize exposure of each individual area of the retina. To prevent loss of data quality it is recommended to restrict analysis to areas in which there is effectively single stratification of the capillary bed, for example in the region immediately surrounding the foveal avascular zone.

An important step in the application of PIV to our data was the rejection of spurious individual velocity measurements, based on presumed physiological constraints on erythrocyte speed and the direction of flow. However under the influence of disease and age, there is potential for marked slowing or acceleration of erythrocyte velocity and/or the formation of abnormal capillary geometry (e.g. micro-aneurysms, anastomoses). This may necessitate that outliers be identified by statistical methods [57–58], rather than preconceptions of the likely range of values. Beyond these limitations, data acquisition will be limited in ways typical for flood adaptive optics imaging in general, namely by the presence of scattering media and small pupils in the aged eye, poor fixation, or large amounts of higher order aberrations that are not well corrected by the deformable mirror. Data from more subjects are required to evaluate the influence of aged, diseased or otherwise difficult eyes on the approach detailed here.

The PIV and division [38] approaches discussed above successfully identified the majority of capillary segments in our sequences. However the signal to noise ratio was observed to be low in several capillary segments in which motion was nonetheless subjectively identified with relative ease. This was especially true in regions that approached branch points and neighboring vessels. While the reliability of such subjective analysis is debatable, it is possible that approaches can be borrowed from investigations of complex human motion perception and used to more accurately characterize the blood flow statistics of these relatively low contrast data sets.

5. Conclusions

We have devised a method to directly and noninvasively visualize erythrocytes flowing in single file in capillaries in the living human eye. The method lends itself well to particle image velocimetry for the quantification of erythrocyte velocity, which has confirmed high

#175393 - $15.00 USD Received 31 Aug 2012; revised 8 Oct 2012; accepted 13 Nov 2012; published 15 Nov 2012

spatiotemporal variability in flow of erythrocytes in retinal capillaries. Our method complements other tools for the assessment of blood flow in the retina, which include assessment of retinal leukocyte dynamics [25,26], erythrocyte flow profiles in arterioles and venules [31,32], and velocity in the larger retinal vessels via Doppler/speckle measurement [14–16]. Together these tools allow the noninvasive study of flow dynamics in retinal vessels of any caliber in the living human eye, which has important ramifications not only for study of retinal disease but also for diseases of the cerebrovascular and cardiovascular systems.

Acknowledgments

This project was supported by an Australian Research Council Discovery Early Career Researcher Award (DE120101931), an Australia Research Council Discovery Project Grant (DP0984649), an A.E. Rowden White Foundation benevolent bequest, and the University of Melbourne Interdisciplinary Seed Fund.

#175393 - $15.00 USD Received 31 Aug 2012; revised 8 Oct 2012; accepted 13 Nov 2012; published 15 Nov 2012